

# A Unified Dynamic Characterization Framework for Microgrid Systems

BRIAN JOHNSON,<sup>1</sup> ALI DAVOUDI,<sup>2</sup> PATRICK CHAPMAN,<sup>3</sup>  
and PETER SAUER<sup>1</sup>

<sup>1</sup>Electrical and Computer Engineering Department, University of Illinois  
at Urbana-Champaign, Urbana, Illinois, USA

<sup>2</sup>Department of Electrical Engineering, University of Texas at Arlington,  
Arlington, Texas, USA

<sup>3</sup>SolarBridge Technologies, Austin, Texas, USA

**Abstract** *A systematic, automatable, unified methodology is presented for the modeling of non-linear large-signal dynamics and eigenvalue analysis of microgrid systems. Unlike nodal-based simulators and typical state-variable methods that require Kirchhoff's current law analysis, a state-space model is systematically derived from the netlist of the equivalent qd microgrid circuit model. The model may be used to conduct time-domain simulations and analyze system response to large transients. Additionally, system eigenvalues may be analyzed with respect to inverter control gains and system parameters to assess small-signal stability and sensitivity. The dynamic model is verified against existing experimental results, and small-signal stability results are presented.*

**Keywords** microgrid, power system dynamics, power system stability, simulation, power system control

## 1. Introduction

A unified formulation for analyzing the large-signal transient response and small-signal stability of microgrid power systems is presented. A microgrid, defined as a controllable electrical network containing distributed energy sources and storage devices, connected to the main grid through a bypass switch, is capable of islanding from the grid utility to provide uninterrupted power to local loads [1]. Microgrids are often employed in mission-critical applications, such as medical, military, and telecommunication installations. A variety of distributed resources and storage devices, such as photovoltaics, wind, fuel cells, gas turbines, flywheels, and batteries, can be integrated into the system [2]. An overview of various existing microgrid installations and their respective characteristics can be found in [3, 4].

Several types of microgrids have been analyzed: rectifier-based DC microgrids [5, 6], mixed systems of AC machines and inverters in AC microgrids [7–9], and inverter-based

Received 2 March 2011; accepted 5 September 2011.

Address correspondence to Brian Johnson, Electrical and Computer Engineering Department, University of Illinois at Urbana-Champaign, 335 Everitt Lab. Bldg., 1406 West Green Street, Urbana, IL 61821. E-mail: johnso88@illinois.edu

AC microgrids [10–15]. Significant effort has been conducted in droop-based control design [16–23] and small-signal stability analysis [24, 25] of inverter-based microgrids. For system analysis, a dynamic model must first be established. It is preferable that the model formulation be general, systematic, and able to be automated.

Two distinct approaches have been employed to formulate microgrid dynamic models. For the first approach, a numerical integration method is used to express the network state equations as a set of algebraic difference equations. Consequently, the network can be represented as a linear system of resistors and current sources at each time step. This approach, as outlined in [26–30], can be used to study the time-domain transient response of a microgrid under disturbances, such as islanding, load changes, and faults. Examples of available transient simulators include electromagnetic transients program (EMTP), alternative transient program (ATP), power systems computer-aided design (PSCAD), and, most recently, real-time digital simulator (RTDS) technologies.

Alternatively, a state-variable-based approach can be implemented once differential equations are attained. The analytical state-variable formulation allows the use of many control design and small-signal analysis techniques (*e.g.*, eigenvalue analysis, feedback linearization) [26, 30, 31]. A detailed treatment of model formulation and small-signal stability analysis of power systems was outlined in [32, 33]. Despite the opportunity for system analysis, the formulation of differential equations for dynamic systems can be tedious. Although a microgrid is relatively small in size in comparison to large-scale power systems, the number of equations associated with the controllers and network can make an explicit formulation time consuming. The existing methods for establishing network state equations generally require the analyst to evaluate Kirchhoff's current law (KCL) at each network node [8, 9, 25]. And circuit components, such as transformers and mutual coupling [25], are often discarded to simplify model formulation. An efficient method for establishing state equations without KCL analysis is preferred.

An automated methodology for dynamic characterization of inverter-based microgrids that allows for analysis of both time-domain transient behavior and small-signal stability is utilized in this article. The modeling technique will be used to analyze the behavior of the Consortium for Electric Reliability Technology Solutions (CERTS) microgrid. Previous work in modeling the CERTS microgrid has predominantly focused on EMTP-based transient models [34–36]. Because little work has been devoted toward developing a CERTS microgrid model for eigenvalue analysis, one main contribution of this article will be a model capable of small-signal stability analysis of the CERTS system. The proposed formulation is general and can be applied to a variety of inverter-based microgrids. Commonly used microgrid components, such as voltage sources, loads, transmission lines, and transformers, are represented in the quadrature and direct ( $qd$ ) axes. Using the given network topology and parameters with the equivalent  $qd$  circuit, the automated state model generation (ASMG) algorithm is employed to derive a state-space model. The fundamental principles of the ASMG method are outlined in [37, 38]. Non-linear dynamics can be included since the proposed dynamic model formulation does not require linearization. After the closed-loop equations are formulated, eigenvalue analysis can be used to assess the relationship between control and circuit parameters with system stability. The ASMG method, which has mainly been applied to motor drives [37, 39], is extended to microgrid applications in order to study both dynamics and stability.

This article is structured as follows: Section 2 gives a brief overview of the CERTS microgrid characteristics and control. A general approach for producing the equivalent  $qd$  network and its associated state-space model is shown in Section 3. Section 4 establishes

closed-loop system equations. Section 5 gives case studies of the CERTS system, and Section 6 is the conclusion.

## 2. Microgrid Characteristics and Control

The proposed technique will be used to analyze the CERTS microgrid and its associated control. AC energy sources are rectified, and DC energy sources interface with a DC-DC converter before being connected to a DC bus. Then, local DC buses are interfaced to the microgrid AC bus using parallel inverters. For the purpose of modeling inverter AC output and system level dynamics, the DC bus voltage magnitude is assumed to be fixed because it varies slowly. The inverter may be modeled as a controllable AC voltage source with output  $\mathbf{e}_{inv(abc)}$ , as the inverter switching frequency of 4 kHz is much greater than the AC line frequency [7, 23–25, 30, 40]. The output voltage  $\mathbf{e}_{inv(abc)}$  has magnitude  $E_{inv}$  and phase  $\theta_{inv}$  with respect to the microgrid system AC bus. The inverter is interfaced to the bus through an LCL filter and a three-phase transformer, as shown in Figure 1.

Assuming that the effective reactance of the LCL filter  $X$  is purely inductive, the real and reactive power exported from the inverter during steady-state conditions can be expressed as [1, 10, 36] as

$$P = \frac{E_{inv}V}{X} \sin \theta_{inv}, \quad (1)$$

$$Q = \frac{E_{inv}V}{X} \cos \theta_{inv} - \frac{V^2}{X}. \quad (2)$$

As the inverter phase angle is typically small,  $P$  is proportional to  $\theta_{inv}$ , and  $Q$  is proportional to  $E_{inv}$ . Thus, the inverter can be used to control the real and reactive power injected into the microgrid bus. A droop controller is implemented such that the inverter mimics the inertia of a synchronous machine. This ensures autonomous inverter operation and minimizes system-level communication [17, 18, 41]. Using the relationships established in Eqs. (1) and (2), the inverter frequency and voltage magnitude are controlled to satisfy

$$\omega = \omega_s - m_P(P - P^*), \quad (3)$$

and

$$E_{inv} = V^* - m_Q Q. \quad (4)$$

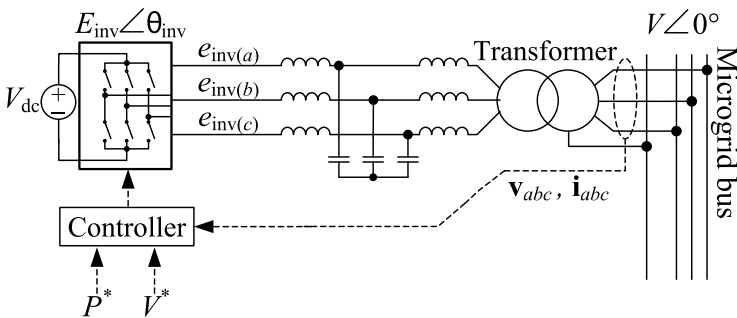


Figure 1. Inverter configuration and closed-loop control.

Generally, Eqs. (3) and (4) are referred to as the  $P$ - $\omega$  and  $Q$ - $V$  droop equations, respectively. In Eqs. (3) and (4),  $V^*$  and  $P^*$  are the bus voltage magnitude and power commands, respectively. The synchronous frequency is denoted as  $\omega_s$ . During grid-connected operation, each inverter will behave as a current source and regulate the power injected into the microgrid such that  $P = P^*$ . While islanded, the inverters support the microgrid voltage and adjust their respective power outputs to share the microgrid load. Under islanded conditions, the microgrid will approach a steady-state frequency  $\omega$ , where possibly  $\omega \neq \omega_s$  [17, 18, 23].

The CERTS microgrid uses a droop controller, which adheres to the above principles except that the  $Q$ - $V$  droop utilizes a proportional-integral (PI) controller [40]. The voltage control law can be expressed as

$$E_{inv} = K_p(V_{set} - V) + K_i \int V_{set} - V dt, \quad (5)$$

where  $V_{set} = V^* - m_Q Q$ . The AC bus voltage and current measurements, as shown in Figure 1, are denoted as  $\mathbf{v}_{abc}$  and  $\mathbf{i}_{abc}$ , respectively. The controller output commands  $E_{inv}$  and  $\theta_{inv}$  are used to generate the pulse-width modulation (PWM) gate signals such that the inverter voltage output satisfies

$$\mathbf{e}_{inv(abc)} = E_{inv} \begin{bmatrix} \cos(\theta_{inv}) \\ \cos\left(\theta_{inv} - \frac{2\pi}{3}\right) \\ \cos\left(\theta_{inv} + \frac{2\pi}{3}\right) \end{bmatrix}. \quad (6)$$

The inverter controller differential equations are summarized in Eqs. (7)–(11):

$$\frac{d}{dt}P = \frac{\tilde{P} - P}{\tau_P}, \quad (7)$$

$$\frac{d}{dt}Q = \frac{\tilde{Q} - Q}{\tau_Q}, \quad (8)$$

$$\frac{d}{dt}V = \frac{\tilde{V} - V}{\tau_V}, \quad (9)$$

$$\frac{d}{dt}\theta_{inv} = \omega_s - m_P(P - P^*), \quad (10)$$

$$\frac{d}{dt}z = K_i(V^* - m_Q Q - V), \quad (11)$$

$$\tilde{P} = \frac{3}{2}(v_d i_d + v_q i_q), \quad (12)$$

$$\tilde{Q} = \frac{3}{2}(v_d i_q - v_q i_d), \quad (13)$$

$$\tilde{V} = \sqrt{v_d^2 + v_q^2}, \quad (14)$$

where  $\mathbf{v}_{qd} = [v_q \ v_d]^T$  and  $\mathbf{i}_{qd} = [i_q \ i_d]^T$  are the transformed measurements  $\mathbf{v}_{abc}$  and  $\mathbf{i}_{abc}$ . The states  $P$ ,  $Q$ , and  $V$  are the filtered power, reactive power, and voltage calculations, respectively, and  $z$  is the integrator output in the  $Q$ - $V$  droop PI controller. The output voltage of every inverter, as expressed in Eq. (6), can be written in terms of its controller states. The inverter voltage magnitude, as expressed in Eq. (5), can be rewritten as

$$E_{inv} = z + K_p(V^* - m_Q Q - V). \quad (15)$$

Zero-axis quantities are neglected, as the system is assumed to be balanced. It should be noted that the inverter control equations in Eqs. (7)–(11) are non-linear due to the calculations in Eqs. (12)–(14). Furthermore, non-linearities are introduced by the power limits of the inverter. Each inverter controller has a total of five state variables.

The microgrid typically contains multiple inverters; notation must be established for system-level analysis.  $\mathbf{x}_{inv}$  is defined as a vector containing all inverter controller states. Given a system with  $m$  inverters,

$$\mathbf{x}_{inv} = \begin{bmatrix} \mathbf{x}_{inv(1)} \\ \vdots \\ \mathbf{x}_{inv(m)} \end{bmatrix}. \quad (16)$$

In Eq. (16), each entry  $\mathbf{x}_{inv(i)}$  is a vector comprised of states  $P$ ,  $Q$ ,  $V$ ,  $\theta_{inv}$ , and  $z$  of the  $i$ th inverter. Similarly, the non-linear state equations of the multiple inverter controllers can be written succinctly as

$$\frac{d}{dt}\mathbf{x}_{inv} = \frac{d}{dt} \begin{bmatrix} \mathbf{x}_{inv(1)} \\ \vdots \\ \mathbf{x}_{inv(m)} \end{bmatrix} = \mathbf{f}_{inv}(\mathbf{x}_{inv}, \mathbf{v}_{br}, \mathbf{i}_{br}), \quad (17)$$

where each entry  $\frac{d}{dt}\mathbf{x}_{inv(i)}$  is a vector with the differential equations in Eqs. (7)–(11) of the  $i$ th inverter controller. Since the state equations of each controller depend on measurement signals, as shown in Figure 1, Eq. (17) is written as a function of the microgrid network voltages and currents  $\mathbf{v}_{br}$  and  $\mathbf{i}_{br}$ , respectively.

### 3. Network Model

The equivalent  $qd$  circuit network equations are formulated, which yield constant values in the steady-state, unlike the original  $abc$  circuit. This property will facilitate linearization and small-signal stability analysis. Using the ASMG algorithm, a systematic method of formulating the state-space model of the microgrid network will be established such that the analyst is relieved of explicitly deriving the circuit differential equations.

### 3.1. Park's Transformation of Circuit Components

Park's transformation, as defined in Eq. (18), is used to transform a set of three-phase variables,  $\mathbf{f}_{abc}$ , to  $qd0$  quantities,  $\mathbf{f}_{qd0}$ , as shown in Eq. (19):

$$\mathbf{K}_s = \frac{2}{3} \begin{bmatrix} \cos \theta & \cos \left( \theta - \frac{2\pi}{3} \right) & \cos \left( \theta + \frac{2\pi}{3} \right) \\ \sin \theta & \sin \left( \theta - \frac{2\pi}{3} \right) & \sin \left( \theta + \frac{2\pi}{3} \right) \\ \frac{1}{2} & \frac{1}{2} & \frac{1}{2} \end{bmatrix}, \quad (18)$$

$$\mathbf{f}_{qd0} = \mathbf{K}_s \mathbf{f}_{abc}, \quad (19)$$

where  $\theta$  represents the reference frame position and can be expressed as  $\theta = \int \omega_{ref} dt + \theta_i$ , where  $\omega_{ref}$  is the reference frame speed and  $\theta_i$  is the initial position [40]. For the remaining analysis, the synchronous reference frame is used such that  $\theta = \omega_s t$ .

To complete the microgrid network model, only four types of balanced three-phase circuit components are needed: voltage sources, capacitive elements, conductors with series resistance and inductance, and magnetically coupled circuits. Using variations of these fundamental circuit building blocks, it is possible to model transmission lines, three-phase transformers, inverter voltage sources, filtering components, loads, and the infinite bus. Each block will be transformed to an equivalent  $qd$  circuit representation.

**3.1.1. Voltage Sources.** The balanced  $abc$  voltage sources are transformed by applying Park's transformation to the expression for  $\mathbf{v}_{abc}$ . Evaluating  $\mathbf{v}_{qd0} = \mathbf{K}_s \mathbf{v}_{abc}$  in the synchronous reference frame and omitting the zero-axis gives

$$\begin{bmatrix} v_q \\ v_d \end{bmatrix} = V_{pk} \begin{bmatrix} \cos(\theta_e - \omega_s t) \\ -\sin(\theta_e - \omega_s t) \end{bmatrix}, \quad (20)$$

where  $V_{pk}$  is the line-neutral peak voltage amplitude, and  $\theta_e$  is the voltage angle. Equation (20) can be represented as an equivalent  $qd$  circuit [40]. This general result can be used to model the inverter voltage outputs and the infinite bus voltage.

The infinite bus is assumed to operate at a fixed frequency  $\omega_s$  with voltage amplitude  $V_{inf(pk)}$ . Rewriting Eq. (20) such that  $V_{pk} = V_{inf(pk)}$  and  $\theta_e = \omega_s t$ , the infinite bus voltage  $\mathbf{e}_{inf(qd)}$  can be expressed as

$$\begin{bmatrix} e_{inf(q)} \\ e_{inf(d)} \end{bmatrix} = \begin{bmatrix} V_{inf(pk)} \\ 0 \end{bmatrix}, \quad (21)$$

Similarly, the balanced inverter voltages in Eq. (6) may be rewritten as

$$\begin{bmatrix} e_{inv(q)} \\ e_{inv(d)} \end{bmatrix} = E_{inv} \begin{bmatrix} \cos(\theta_{inv} - \omega_s t) \\ -\sin(\theta_{inv} - \omega_s t) \end{bmatrix}. \quad (22)$$

3.1.2. *Capacitive Branches.* Evaluating KCL and applying Park's transformation to a balanced three-phase configuration of capacitors yields

$$\mathbf{i}_{qd0} = C \left( \frac{d}{dt} \mathbf{v}_{qd0} + \mathbf{K}_s \frac{d}{dt} \mathbf{K}_s^{-1} \mathbf{v}_{qd0} \right). \quad (23)$$

It can be shown that the factor  $\mathbf{K}_s \frac{d}{dt} \mathbf{K}_s^{-1}$  reduces to

$$\mathbf{K}_s \frac{d}{dt} \mathbf{K}_s^{-1} = \omega_s \begin{bmatrix} 0 & 1 & 0 \\ -1 & 0 & 0 \\ 0 & 0 & 0 \end{bmatrix}. \quad (24)$$

Substituting Eq. (24) into Eq. (23) and expanding yields

$$\begin{bmatrix} i_q \\ i_d \end{bmatrix} = \begin{bmatrix} C \frac{d}{dt} v_q + \omega_s C v_d \\ C \frac{d}{dt} v_d - \omega_s C v_q \end{bmatrix}, \quad (25)$$

which can be used to formulate the  $qd$  circuit in Figure 2 [40] used to model the inverter filtering capacitors shown in Figure 1.

3.1.3. *Resistive and Inductive Branches.* Given a balanced configuration of RL transmission lines, the analysis of Kirchoff's voltage law (KVL) and application of Eq. (19) yields

$$\mathbf{v}_{qd0} = r \mathbf{i}_{qd0} + L \left( \frac{d}{dt} \mathbf{i}_{qd0} + \mathbf{K}_s \frac{d}{dt} \mathbf{K}_s^{-1} \mathbf{i}_{qd0} \right). \quad (26)$$

Substituting Eq. (24) into Eq. (26) gives

$$\begin{bmatrix} v_q \\ v_d \end{bmatrix} = \begin{bmatrix} r i_q + L \frac{d}{dt} i_q + \omega_s L i_d \\ r i_d + L \frac{d}{dt} i_d - \omega_s L i_q \end{bmatrix}, \quad (27)$$

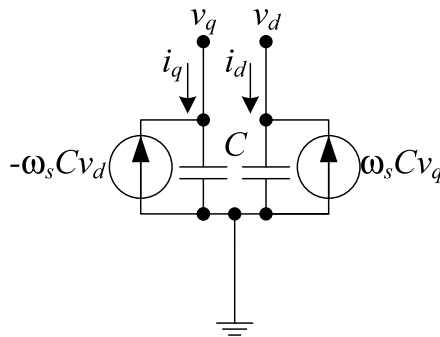


**Figure 2.** Equivalent  $qd$  circuitry of three-phase capacitor configuration.

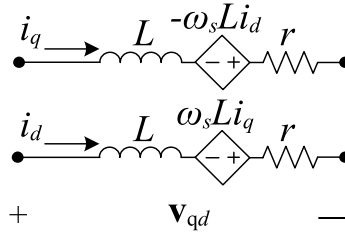


**Figure 3.** Equivalent  $qd$  circuitry of three-phase RL circuit.

which can be represented using the RL circuit in Figure 3 [40]. In addition, purely resistive and inductive circuits can be represented using Eq. (27) by setting  $L$  or  $r$  to zero.

**3.1.4. Magnetically Coupled Circuits.** Each inverter and the infinite bus in the CERTS microgrid are connected to a 480-V/208-V step-down transformer. The transformer is modeled as three pairs of inductively coupled circuits connected in the grounded wye-wye configuration. Figure 4 shows the  $abc$  transformer model. After evaluating KVL and applying Park's transformation, Eqs. (28) and (29) describe the primary and secondary coils of the transformer, respectively. Expanding Eqs. (28) and (29) and omitting the zero-axis, the transformer can be represented by the equivalent circuit in Figure 4;

$$\mathbf{v}_{qd01} = r_1 \mathbf{i}_{qd01} + L_1 \left( \frac{d}{dt} \mathbf{i}_{qd01} + \mathbf{K}_s \frac{d}{dt} \mathbf{K}_s^{-1} \mathbf{i}_{qd01} \right) + M \left( \frac{d}{dt} \mathbf{i}_{qd02} + \mathbf{K}_s \frac{d}{dt} \mathbf{K}_s^{-1} \mathbf{i}_{qd02} \right), \quad (28)$$

$$\mathbf{v}_{qd02} = r_2 \mathbf{i}_{qd02} + L_2 \left( \frac{d}{dt} \mathbf{i}_{qd02} + \mathbf{K}_s \frac{d}{dt} \mathbf{K}_s^{-1} \mathbf{i}_{qd02} \right) + M \left( \frac{d}{dt} \mathbf{i}_{qd01} + \mathbf{K}_s \frac{d}{dt} \mathbf{K}_s^{-1} \mathbf{i}_{qd01} \right). \quad (29)$$

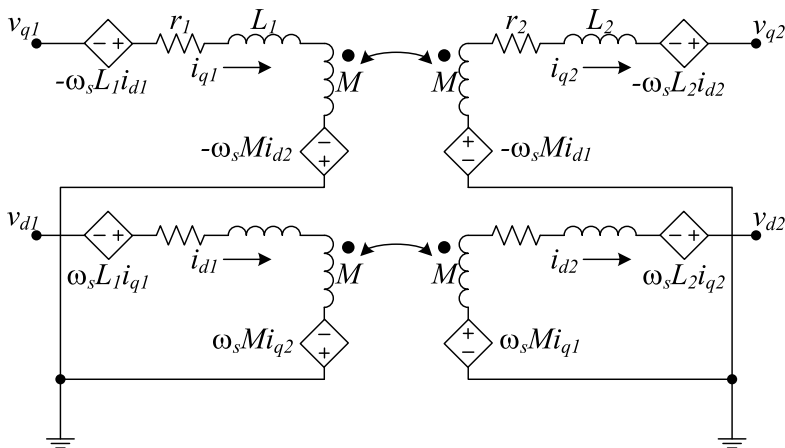


**Figure 4.** Equivalent  $qd$  circuitry of three-phase transformer.

### 3.2. Automated State-space Model Formulation

Once the  $qd$ -axes network circuit has been established, the circuit state equations must be formulated. The microgrid is represented as a collection of  $n$  nodes and  $b$  branches using a directed graph. Each branch is a variation of the elementary model shown in Figure 5. All of the microgrid circuit branches can be constructed by setting appropriate parameters to zero. Using the additional capability that the voltage and current sources  $e_i$  and  $j_i$  can be functions of time and other variables, all the equivalent  $qd$  branches, and the voltage-source inverter model may be represented by this elementary branch.

The interconnected branches form the microgrid network whose structure is described by the  $b \times n$  node-incidence matrix  $\mathbf{A}_a$ . Each column corresponding to a branch will have exactly two non-zero entries, with one equal to  $+1$  and the other to  $-1$ . The  $+1$  entry at the  $(i, j)$  entry of matrix  $\mathbf{A}_a$  indicates the positive terminal connection of the  $j$ th branch to the  $i$ th node. The  $-1$  entry corresponds to the negative terminal connection. After row operations, matrix  $\mathbf{A}_a$  may be expressed [26, 37] as Eq. (30):

$$\tilde{\mathbf{A}}_a = \begin{bmatrix} \mathbf{I}_{(n-1) \times (n-1)} & \hat{\mathbf{A}}_{(n-1) \times (b-n+1)} \\ \mathbf{0}_{1 \times (n-1)} & \mathbf{0}_{1 \times (b-n+1)} \end{bmatrix}. \quad (30)$$

Defining  $P_i = 1/C_i$ , the parameters of each branch  $r_i$ ,  $L_i$ , and  $P_i$  constitute  $b \times b$  matrices  $\mathbf{R}_{br}$ ,  $\mathbf{L}_{br}$ , and  $\mathbf{P}_{br}$ , respectively. If a branch contains no capacitance,  $P_i = 0$ .  $\mathbf{M}$  is a  $b \times b$  matrix whose entries  $m_{i,j} = 1$  if the  $j$ th capacitor is connected to the  $i$ th branch and zero otherwise. The sources  $e_i$  and  $j_i$  form  $b$ -dimensional vectors  $\mathbf{e}_{br}$  and  $\mathbf{j}_{br}$ , respectively. The off-diagonal elements in the inductance matrices represent mutual coupling between branches and may be utilized to model transformers commonly used in microgrid power systems. Defining  $\mathbf{v}_{br}$ ,  $\mathbf{i}_{br}$ , and  $\mathbf{q}_{br}$  as the vectors containing the branch voltages, currents, and capacitor charges, respectively, the branch voltages may be expressed [37] as

$$\mathbf{v}_{br} = \mathbf{R}_{br} \mathbf{i}_{br} + \frac{d}{dt} (\mathbf{L}_{br} \mathbf{i}_{br}) + \mathbf{P}_{br} \mathbf{q}_{br} + \mathbf{e}_{br}, \quad (31)$$

where

$$\mathbf{q}_{br} = \frac{d}{dt} (\mathbf{i}_{br} + \mathbf{j}_{br}). \quad (32)$$

As demonstrated in [37], the voltage expression in Eq. (31) can be manipulated using a series of algebraic steps to create a state-space model, as in Eqs. (33) and (34), of the

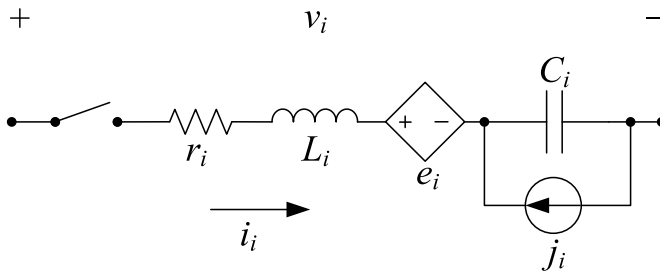


Figure 5. Elementary branch model.

microgrid network:

$$\frac{d}{dt} \begin{bmatrix} \mathbf{q}_c \\ \mathbf{i}_x \end{bmatrix} = \begin{bmatrix} \mathbf{0} & \mathbf{M}^T \mathbf{B}_b^T \\ -\mathbf{L}_x^{-1} \mathbf{P}_x & -\mathbf{L}_x^{-1} \left( \mathbf{r}_x + \frac{d}{dt} \mathbf{L}_x \right) \end{bmatrix} \begin{bmatrix} \mathbf{q}_c \\ \mathbf{i}_x \end{bmatrix} + \begin{bmatrix} \mathbf{M}^T & \mathbf{0} \\ \mathbf{0} & -\mathbf{L}_x^{-1} \mathbf{B}_b \end{bmatrix} \begin{bmatrix} \mathbf{j}_{br} \\ \mathbf{e}_{br} \end{bmatrix}, \quad (33)$$

$$\begin{bmatrix} \mathbf{i}_{br} \\ \mathbf{v}_{br} \end{bmatrix} = \begin{bmatrix} \mathbf{0} & \mathbf{B}_b^T \\ \mathbf{P}_{br} \mathbf{M} - \mathbf{L}_{br} \mathbf{B}_b^T \mathbf{L}_x^{-1} \mathbf{P}_x & \left( \mathbf{r}_{br} + \frac{d}{dt} \mathbf{L}_{br} \right) \mathbf{B}_b^T - \mathbf{L}_{br} \mathbf{B}_b^T \mathbf{L}_x^{-1} \left( \mathbf{r}_x + \frac{d}{dt} \mathbf{L}_x \right) \end{bmatrix} \cdot \begin{bmatrix} \mathbf{q}_c \\ \mathbf{i}_x \end{bmatrix} + \begin{bmatrix} \mathbf{0} & \mathbf{0} \\ \mathbf{0} & \mathbf{I} - \mathbf{L}_{br} \mathbf{B}_b^T \mathbf{L}_x^{-1} \mathbf{B}_b \end{bmatrix} \begin{bmatrix} \mathbf{j}_{br} \\ \mathbf{e}_{br} \end{bmatrix}. \quad (34)$$

The matrices  $\mathbf{B}_b$ ,  $\mathbf{q}_c$ ,  $\mathbf{r}_x$ ,  $\mathbf{L}_x$ , and  $\mathbf{P}_x$  are defined in Eqs. (35)–(39):

$$\mathbf{B}_b^T = \begin{bmatrix} \hat{\mathbf{A}} \\ \mathbf{I}_{(b-n+1) \times (b-n+1)} \end{bmatrix}, \quad (35)$$

$$\mathbf{q}_c = \mathbf{M}^T \mathbf{q}_{br}, \quad (36)$$

$$\mathbf{r}_x = \mathbf{B}_b \mathbf{r}_{br} \mathbf{B}_b^T, \quad (37)$$

$$\mathbf{L}_x = \mathbf{B}_b \mathbf{L}_{br} \mathbf{B}_b^T, \quad (38)$$

$$\mathbf{P}_x = \mathbf{B}_b \mathbf{P}_{br} \mathbf{B}_b^T. \quad (39)$$

As machine dynamics are not modeled, all circuit inductances will be constant such that  $\frac{d}{dt} \mathbf{L}_x = \frac{d}{dt} \mathbf{L}_{br} = \mathbf{0}$  in Eq. (34). Consequently, the state matrices will be constant valued. For compactness, Eqs. (33) and (34) may be written as

$$\frac{d}{dt} \mathbf{x}_{net} = \mathbf{A} \mathbf{x}_{net} + \mathbf{B} \mathbf{u} \quad (40)$$

and

$$\mathbf{y} = \mathbf{C} \mathbf{x}_{net} + \mathbf{D} \mathbf{u}, \quad (41)$$

where  $\mathbf{x}_{net} = [\mathbf{q}_c \ \mathbf{i}_x]^T$  is a vector of the state variables,  $\mathbf{u} = [\mathbf{j}_{br} \ \mathbf{e}_{br}]^T$  is a vector of the current and voltage sources, and  $\mathbf{y} = [\mathbf{i}_{br} \ \mathbf{v}_{br}]^T$  contains all branch currents and voltages. The matrices  $\mathbf{A}$ ,  $\mathbf{B}$ ,  $\mathbf{C}$ , and  $\mathbf{D}$  can be defined by inspection of Eqs. (33) and (34).

The advantage of the presented formulation is that the network differential equations can be defined systematically using the network circuit parameters and topology. Thus, the analyst need not explicitly derive numerous state equations of a possibly complex network. Additionally, by updating the node-incidence matrix  $\mathbf{A}_a$ , the ASMG method can be used to model systems with dynamic topologies. This capability allows for simulation of microgrid islanding transients and other switching events.

#### 4. Formulation of Closed-loop Equations

The closed-loop state equations must be expressed before the system can be linearized for stability analysis. In this context, the inverter control equations of Section 2 form the feedback loop, and the network state-space model of Section 3 represents the plant. The closed-loop system state equations will be expressed in the form

$$\frac{d}{dt}\tilde{\mathbf{x}} = \mathbf{f}_{\text{sys}}(\tilde{\mathbf{x}}), \quad (42)$$

where  $\mathbf{f}_{\text{sys}}(\tilde{\mathbf{x}})$  is non-linear, and  $\tilde{\mathbf{x}}$  contains both the inverter control and network state variables  $\mathbf{x}_{\text{inv}}$  and  $\mathbf{x}_{\text{net}}$ , respectively.  $\tilde{\mathbf{x}}$  is defined as

$$\tilde{\mathbf{x}} = \begin{bmatrix} \mathbf{x}_{\text{net}} \\ \mathbf{x}_{\text{inv}} \end{bmatrix}. \quad (43)$$

For the closed-loop state equations to be expressed in the form shown in Eq. (42), a series of algebraic substitutions will be made as outlined below.

- The vector  $\mathbf{u}$  containing the network voltage and current source outputs can be written as a function of the states,  $\mathbf{u} = \mathbf{f}_u(\tilde{\mathbf{x}})$ .
- The network and inverter control differential equations can be expressed as  $\frac{d}{dt}\mathbf{x}_{\text{net}} = \mathbf{f}_{\text{net}}(\tilde{\mathbf{x}})$  and  $\frac{d}{dt}\mathbf{x}_{\text{inv}} = \mathbf{f}_{\text{inv}}(\tilde{\mathbf{x}})$ .
- Using the result of the previous step, the closed-loop state equations will be written as  $\frac{d}{dt}\tilde{\mathbf{x}} = \mathbf{f}_{\text{sys}}(\tilde{\mathbf{x}})$ .

As shown in Figure 5, a network branch may contain a voltage source  $e_i$  and current source  $j_i$ . The voltage and current sources form the vector  $\mathbf{u} = [\mathbf{j}_{br} \ \mathbf{e}_{br}]^T$  in the network state-space model. Using KCL, all branch currents  $\mathbf{i}_{br}$  may be written in terms of the independent state currents  $\mathbf{i}_x$ :

$$\mathbf{i}_{br} = \mathbf{B}_b^T \mathbf{i}_x. \quad (44)$$

Thus, the current-dependent voltage sources in the inductive branches shown in Figure 3 are state dependent. Next, substituting Eq. (15) into Eq. (22), the inverter voltage source outputs can be written in terms of inverter states  $\mathbf{x}_{\text{inv}}$ . Using these two results, all network voltage sources in vector  $\mathbf{e}_{br}$  are state dependent. For  $\mathbf{u} = [\mathbf{j}_{br} \ \mathbf{e}_{br}]^T$  to be written entirely as a function of the states, it will next be shown that the current sources  $\mathbf{j}_{br}$  are also state dependent.

As illustrated in Figure 2, all capacitive branches contain capacitor-voltage-dependent current sources. Branches containing inverter filter capacitors are modeled as having zero resistance, zero inductance, and no voltage sources. Thus, it is possible to show that by using Eq. (34), the capacitor voltages are equal to the rows corresponding to the capacitive branch indices in the vector  $\mathbf{v}_{\text{cap}} = \mathbf{P}_{br} \mathbf{M} \mathbf{q}_c$ , where  $\mathbf{q}_c$  is a state-variable vector of the capacitor charges. Therefore, all capacitor voltages can be expressed in terms of the state variables in  $\mathbf{q}_c$ , and by extension, the capacitor-voltage dependent current sources also depend on  $\mathbf{q}_c$ . Using the fact that  $\mathbf{e}_{br}$  and  $\mathbf{j}_{br}$  have been shown to be state dependent,  $\mathbf{u}$  can be written as the function

$$\mathbf{u} = \begin{bmatrix} \mathbf{e}_{br} \\ \mathbf{j}_{br} \end{bmatrix} = \mathbf{f}_u(\tilde{\mathbf{x}}). \quad (45)$$

Next, it will be shown how Eq. (45) will be used to formulate the network and control differential equations as  $\frac{d}{dt}\mathbf{x}_{net} = \mathbf{f}_{net}(\tilde{\mathbf{x}})$  and  $\frac{d}{dt}\mathbf{x}_{inv} = \mathbf{f}_{inv}(\tilde{\mathbf{x}})$ . Substituting Eq. (45) into Eq. (40) gives

$$\frac{d}{dt}\mathbf{x}_{net} = \mathbf{A}\mathbf{x}_{net} + \mathbf{B}\mathbf{f}_u(\tilde{\mathbf{x}}) = \mathbf{f}_{net}(\tilde{\mathbf{x}}). \quad (46)$$

As the network state equations have been written as a function of  $\tilde{\mathbf{x}}$ , all that remains is for the inverter control equations  $\mathbf{f}_{inv}(\mathbf{x}_{inv}, \mathbf{v}_{br}, \mathbf{i}_{br})$  to be written in terms of system states. Since the inverter state equations depend on measurements,  $\mathbf{v}_{br}$  and  $\mathbf{i}_{br}$  must be written in terms of the states. Using Eq. (45), all network voltages and currents can be written as

$$\mathbf{y} = \begin{bmatrix} \mathbf{i}_{br} \\ \mathbf{v}_{br} \end{bmatrix} = \mathbf{C}\mathbf{x}_{net} + \mathbf{D}\mathbf{f}_u(\tilde{\mathbf{x}}) = \mathbf{f}_{br}(\tilde{\mathbf{x}}). \quad (47)$$

With this result, Eq. (17) becomes

$$\frac{d}{dt}\mathbf{x}_{inv} = \mathbf{f}_{inv}(\mathbf{x}_{inv}, \mathbf{v}_{br}, \mathbf{i}_{br}) = \mathbf{f}_{inv}(\mathbf{x}_{inv}, \mathbf{f}_{br}(\tilde{\mathbf{x}})) = \mathbf{f}_{inv}(\tilde{\mathbf{x}}). \quad (48)$$

Concatenating Eqs. (46) and (48), the system closed-loop equations are

$$\frac{d}{dt}\tilde{\mathbf{x}} = \frac{d}{dt} \begin{bmatrix} \mathbf{x}_{net} \\ \mathbf{x}_{inv} \end{bmatrix} = \begin{bmatrix} \mathbf{f}_{net}(\tilde{\mathbf{x}}) \\ \mathbf{f}_{inv}(\tilde{\mathbf{x}}) \end{bmatrix} = \mathbf{f}_{sys}(\tilde{\mathbf{x}}). \quad (49)$$

The preceding formulation is general; thus it is applicable to a wide variety of microgrid topologies regardless of the control method. Furthermore, as the steps required to reach the closed-loop form are systematic, the formulation can be automated for computer-aided modeling.

## 5. Case Studies

Simulation of system islanding and grid reconnection is conducted on the CERTS microgrid using the dual-inverter configuration shown in Figure 6. This microgrid system, with parameters summarized in the Appendix, has been verified experimentally in [42]. Here, this physical system is used to verify the large-signal transient modeling technique. Balanced operation is assumed, and all transformers are modeled with grounded wye-wye connections. The loads, rated to consume a total of 18 kW, are purely resistive and modeled as grounded wye connected. The utility grid system is modeled as an infinite bus with an equivalent series impedance. The *qd* circuit model contains 34 branches and 15 nodes;  $b = 34$  and  $n = 15$ . Considering that the model contains  $2b - n + 1 = 54$  network state variables, the model is analytically intractable for practical purposes, and thus, the proposed approach is attractive.

### 5.1. Large-signal Time-domain Studies

Before islanding, the system is utility connected, and both microsources regulate their power output to 0.4 p.u. on a 15-kW base. At  $t = 0.25$  sec in Figure 7, the system is islanded and the two microsources increase their power output to accommodate the total load. Simulation results, shown in Figure 7, closely match measured results from [42].

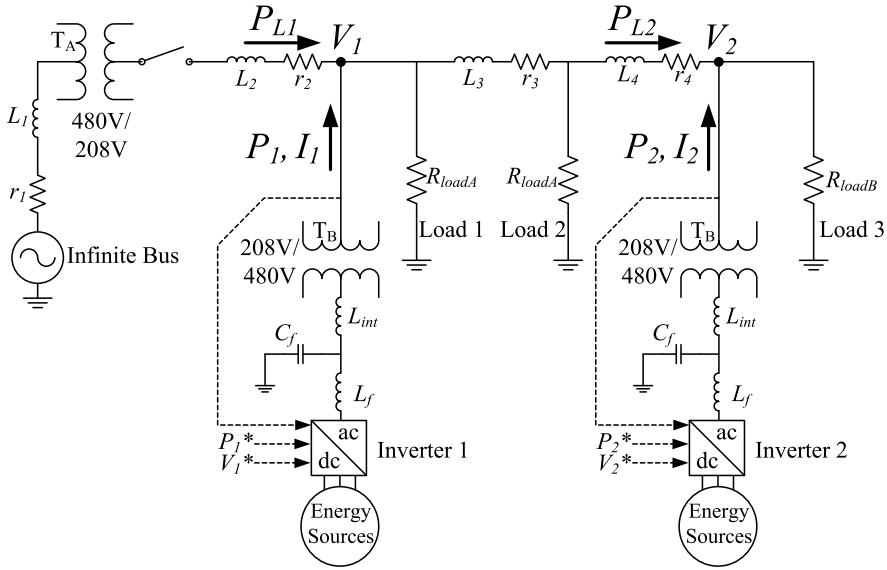


Figure 6. Dual-inverter configuration of CERTS microgrid.

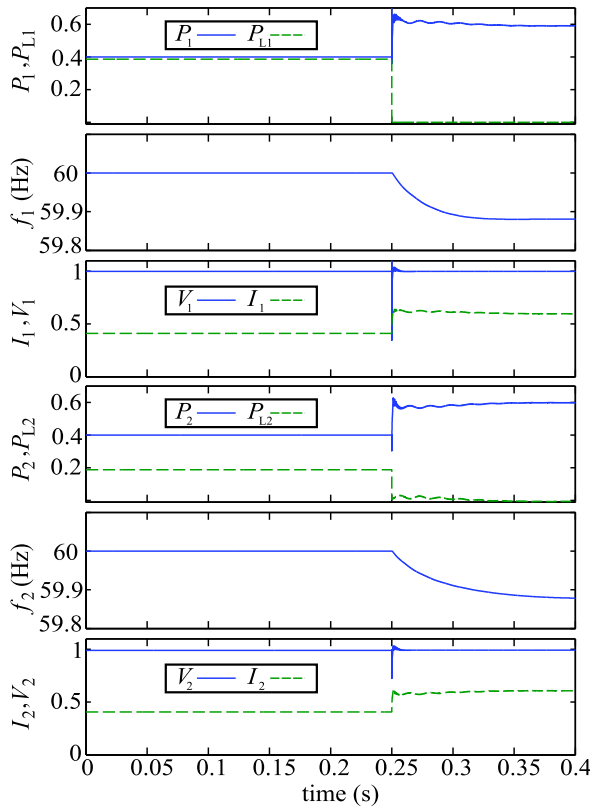
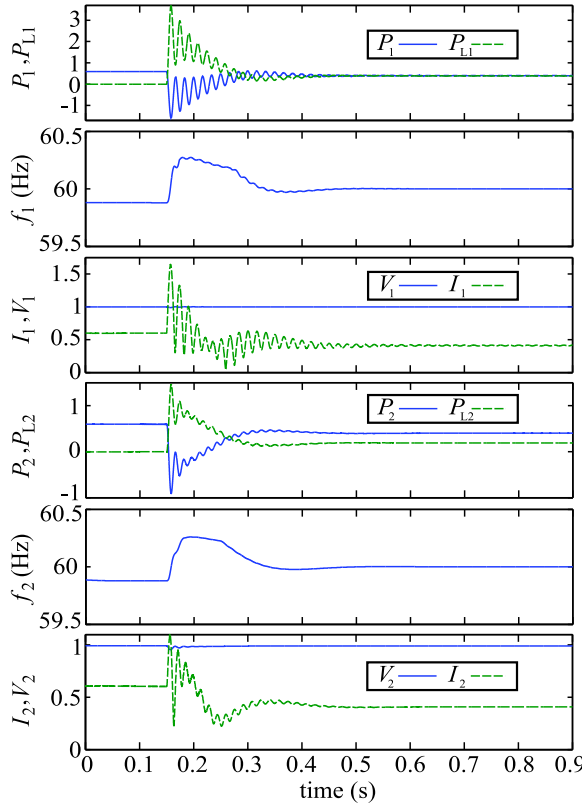


Figure 7. Transient response of inverter 1 and inverter 2 due to system islanding. Power, voltage, and currents are in per unit. (color figure available online)



**Figure 8.** Transient response of inverter 1 and inverter 2 when system is reconnected to the grid utility. Power, voltage, and currents are in per unit. (color figure available online)

These results verify the accuracy of the modeling technique and show that this particular system is stable during islanding.

After the microgrid is islanded and steady-state conditions are reached, the system is reconnected to the utility at  $t = 0.15$  sec, as shown in Figure 8. The inverter controllers then regulate both microsources to produce 0.4 p.u. on a 15-kW base. After system transients subside, the pre-islanding and post-reconnection steady-state conditions are identical.

## 5.2. Small-signal Stability

Linearization may be performed given the closed-loop equations in Eq. (49). Evaluating the Jacobian of  $\mathbf{f}_{sys}(\tilde{\mathbf{x}})$  at the equilibrium points gives the matrix  $\mathbf{A}_{CL}$ . The linearized model is

$$\frac{d}{dt} \Delta \tilde{\mathbf{x}} = \mathbf{A}_{CL} \Delta \tilde{\mathbf{x}}. \quad (50)$$

The system small-signal stability is analyzed by calculating the eigenvalues of  $\mathbf{A}_{CL}$ . The system is unstable when  $\text{Re}(\lambda) > 0$ , for any eigenvalue  $\lambda$ . A root-locus plot of the eigenvalues of  $\mathbf{A}_{CL}$  is generated with respect to the gain settings to determine the relationship between inverter gain settings and stability.

**Table 1**  
Gain setting at system instability

Parameter	Threshold gain when $\text{Re}(\lambda) > 0$
$m_P$	$45.25m_{P(0)}$
$m_{Q1}$	$32.4m_{Q1(0)}$
$m_{Q2}$	$32.4m_{Q2(0)}$

The dual-inverter microgrid shown in Figure 6 is used to illustrate the relationship between the system eigenvalues and controller gains. The former are analyzed under varying control settings, while the system is grid connected and both inverter power outputs are regulated to 6 kW. Specifically, the effect of droop gains  $m_P$  and  $m_Q$  on stability is examined. As each of the control gains is increased, a Hopf bifurcation is encountered, and the system becomes unstable. Table 1 summarizes the minimum gain threshold that produced eigenvalues in the right half of the complex plane. The results are expressed in terms of the typically used base gains  $m_{Q1(0)} = 0.0186$ ,  $m_{Q2(0)} = 0.0215$ , and  $m_{P(0)} = 1.25\pi$ , where  $m_{Q1(0)}$  and  $m_{Q2(0)}$  are the voltage droop gains for inverters 1 and 2, respectively. The frequency droop gain  $m_P$  is identical for both inverters.

The root-locus plot corresponding to the control parameter  $m_Q$  is shown in Figure 9. For clarity, this plot contains the subset of eigenvalues corresponding to the imaginary axis crossing. The power responses of inverter 1 shown in Figure 10 confirm an unstable and growing output for the  $m_Q$  gain setting corresponding to the right-hand plane eigenvalues

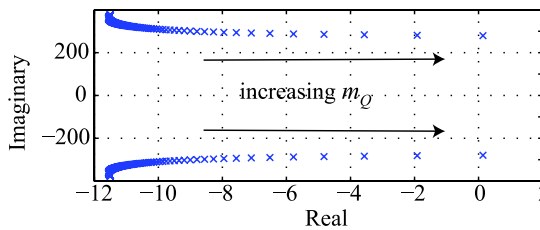


**Figure 9.** Root-locus plot with respect to the gain setting  $m_Q$ . (color figure available online)

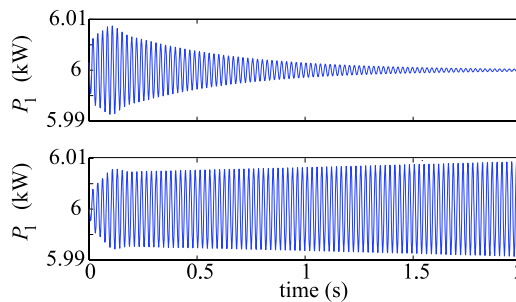


**Figure 10.** Dynamic response of inverter 1: (a) stable operation with voltage-droop gain setting  $m_Q = 32.2m_{Q1(0)}$  and (b) unstable operation with voltage droop gain setting  $m_Q = 32.4m_{Q1(0)}$ . (color figure available online)

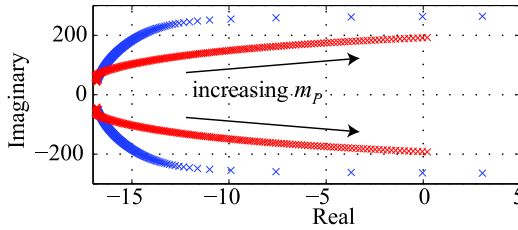


**Figure 11.** Root-locus plot with respect to the gain setting  $m_P$ . (color figure available online)

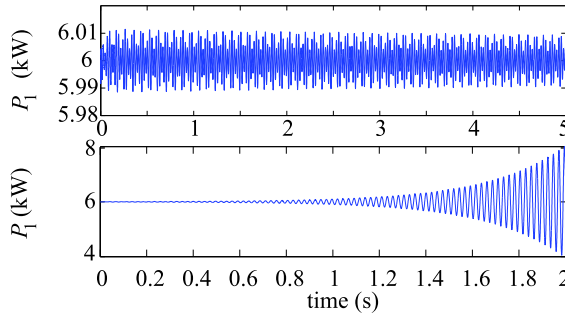


**Figure 12.** Dynamic response of inverter 1: (a) stable operation with frequency-droop gain setting  $m_P = 45m_{P(0)}$  and (b) unstable operation with frequency-droop gain setting  $m_P = 45.25m_{P(0)}$ . (color figure available online)

as summarized in Table 1. When the gain is slightly smaller, the eigenvalues move into the left-hand plane, and correspondingly, the response decays to a bounded output. The dynamic response of inverter 2 is not included but also shows stable and unstable operation corresponding to the eigenvalues in Figure 9.

Next, the root-locus plot with respect to gain  $m_P$  is shown in Figure 11. As in Figure 10, the plot contains only the subset of eigenvalues corresponding to the imaginary axis crossing. The dynamic responses in Figure 12 confirm the findings summarized in Figure 11. They show an exponentially growing output for the  $m_P$  gain setting corresponding to the right-hand plane eigenvalues, as summarized in Table 1. As in the previous case, a smaller gain produces a stable system.

The agreement between the root-locus results and non-linear simulated responses verifies the accuracy of the proposed methodology. Using the demonstrated analysis, a thorough study of the relationship between system parameters and stability can be conducted.

## 6. Conclusion and Future Work

A unified formulation for analyzing the non-linear large-signal transient response and small-signal stability of microgrid power systems was utilized. The microgrid was transformed to an equivalent  $qd$  circuit network such that the state variables are constant in steady-state conditions. An automated state-space model formulation of the network was derived using the node-incidence matrix and circuit parameters. The non-linear inverter control equations and network state-space model were used to derive the system's

closed-loop equations. The resulting non-linear dynamic model, which was verified against existing experimental results for the CERTS microgrid, was utilized to simulate the time-domain system response during an islanding and grid-reconnection transient. After linearizing the closed-loop state equations, the eigenvalues were analyzed with respect to inverter control gains. The proposed model can accommodate non-linear power sources, allowing future work to develop a switching inverter model in which the hex-bridge output voltages are represented as a space-vector in the  $qd0$  domain. DC-bus and storage dynamics could also be incorporated.

## References

1. Lasseter, R., "Microgrids," *Power Eng. Soc. Winter Mtg.*, Vol. 1, pp. 305–308, 2002.
2. Kwasinski, A., and Krein, P., "Multiple-input DC-DC converters to enhance local availability in grids using distributed generation resources," *Applied Power Electronics Conference*, pp. 1657–1663, Anaheim, CA, 25 February 2007.
3. Barnes, M., Kondoh, J., Asano, H., Oyarzabal, J., Ventakaramanan, G., Lasseter, R., Hatziaargriou, N., and Green, T., "Real-world microgrids—an overview," *IEEE International Conference on System of Systems Engineering*, pp. 1–8, San Antonio, TX, 16–18 April 2007.
4. Hatziaargriou, N., Asano, H., Iravani, R., and Marnay, C., "Microgrids," *IEEE Power Energy Mag.*, Vol. 5, pp. 78–94, July–August 2007.
5. Ye, Z., Xing, K., Mazumder, S., Borojevic, D., and Lee, F., "Modeling and control of parallel three-phase PWM boost rectifiers in PEBB-based DC distributed power systems," *Appl. Power Electron. Conf. Expo.*, Vol. 2, pp. 1126–1132, 1998.
6. Feng, X., Liu, C., Ye, Z., Lee, F., and Borojevic, D., "Monitoring the stability of DC distributed power systems," *Annual Conference of the IEEE Industrial Electronics Society*, pp. 1126–1132, San Jose, CA, 29 November–3 December 1999.
7. Deng, W., Tang, X., and Qi, Z., "Research on dynamic stability of hybrid wind/PV system based on micro-grid," *International Conference on Electrical Machines and Systems*, pp. 2627–2632, Wuhan, China, 17–20 October 2009.
8. Katiraei, F., and Iravani, M., "Power management strategies for a microgrid with multiple distributed generation units," *IEEE Trans. Power Syst.*, Vol. 21, pp. 1821–1831, November 2006.
9. Katiraei, F., Iravani, M., and Lehn, P., "Small-signal dynamic model of a micro-grid including conventional and electronically interfaced distributed resources," *IET Generat. Transm. Distrib.*, Vol. 1, pp. 369–378, May 2007.
10. Guerrero, J., de Vicua, L., Matas, J., Castilla, M., and Miret, J., "A wireless controller to enhance dynamic performance of parallel inverters in distributed generation systems," *IEEE Trans. Power Electron.*, Vol. 19, pp. 1205–1213, September 2004.
11. Yu, X., Jiang, Z., and Zhang, Y., "Control of parallel inverter-interfaced distributed energy resources," *IEEE Energy 2030 Conference*, pp. 1–8, Atlanta, GA, 17–18 November 2008.
12. Zhong, Q.-C., Liang, J., Weiss, G., Feng, C., and Green, T., " $H^\infty$  control of the neutral point in four-wire three-phase DC-AC converters," *IEEE Trans. Industrial Electron.*, Vol. 53, pp. 1594–1602, October 2006.
13. Liserre, M., Teodorescu, R., and Blaabjerg, F., "Stability of photovoltaic and wind turbine grid-connected inverters for a large set of grid impedance values," *IEEE Trans. Power Electron.*, Vol. 21, pp. 263–272, January 2006.
14. Blaabjerg, F., Teodorescu, R., Liserre, M., and Timbus, A., "Overview of control and grid synchronization for distributed power generation systems," *IEEE Trans. Industrial Electron.*, Vol. 53, pp. 1398–1409, October 2006.
15. Serban, I., Teodorescu, R., Guerrero, J., and Marinescu, C., "Modeling of an autonomous microgrid for renewable energy sources integration," *Ann. Conf. IEEE Industrial Electron.*, Vol. 1, pp. 4311–4316, 2009.

16. Vasquez, J., Guerrero, J., Luna, A., Rodriguez, P., and Teodorescu, R., "Adaptive droop control applied to voltage-source inverters operating in grid-connected and islanded modes," *IEEE Trans. Industrial Electron.*, Vol. 56, pp. 4088–4096, October 2009.
17. Guerrero, J., Vasquez, J., Matas, J., Castilla, M., and de Vicuna, L., "Control strategy for flexible microgrid based on parallel line-interactive UPS systems," *IEEE Trans. Industrial Electron.*, Vol. 56, pp. 726–736, March 2009.
18. Piagi, P., and Lasseter, R., "Autonomous control of microgrids," *IEEE Power Eng. Soc. Gen. Mtg.*, Vol. 1, pp. 1–8, 2006.
19. Li, Y., Vilathgamuwa, D., and Loh, P., "Design, analysis, and real-time testing of a controller for multibus microgrid system," *IEEE Trans. Power Electron.*, Vol. 19, pp. 1195–1204, September 2004.
20. Cheng, P.-T., Chen, C.-A., Lee, T.-L., and Kuo, S.-Y., "A cooperative imbalance compensation method for distributed-generation interface converters," *IEEE Trans. Industry Appl.*, Vol. 45, pp. 805–815, March 2009.
21. Lee, T.-L., and Cheng, P.-T., "Design of a new cooperative harmonic filtering strategy for distributed generation interface converters in an islanding network," *IEEE Trans. Power Electron.*, Vol. 22, pp. 1919–1927, September 2007.
22. Peng, F., Li, Y., and Tolbert, L., "Control and protection of power electronics interfaced distributed generation systems in a customer-driven microgrid," *IEEE Power Energy Soc. Gen. Mtg.*, Vol. 1, pp. 1–8, 2009.
23. Green, T., and Prodanovic, M., "Control of inverter-based micro-grids," *Elect. Power Syst. Res.*, Vol. 77, pp. 1204–1213, July 2007.
24. Coelho, E., Cortizo, P., and Garcia, P., "Small signal stability for parallel connected inverters in stand-alone AC supply systems," *IEEE Trans. Industry Appl.*, Vol. 38, pp. 533–542, March 2002.
25. Pogaku, N., Prodanovic, M., and Green, T., "Modeling, analysis, and testing of autonomous operation of an inverter-based microgrid," *IEEE Trans. Power Electron.*, Vol. 22, pp. 613–625, March 2007.
26. Chua, L., and Lin, P., *Computer-Aided Analysis of Electronic Circuits: Algorithms and Computational Techniques*, Englewood Cliffs, NJ: Springer, Chap. 1, pp. 46–49, 1975.
27. Singhal, K., and Vlach, J., *Computer Methods for Circuit Analysis and Design*, New York, NY: John Wiley and Sons, Chaps. 1 and 2, pp. 1–58, 1993.
28. Yildiz, A., Cakir, B., Inanc, N., and Abut, N., "A fast simulation technique for the power electronic converters," *Applied Power Electronics Conference and Exposition*, pp. 191–196, Dallas, TX, 14–18 May 1999.
29. Kariniotakis, G., Soutanis, N., Tsouchnikas, A., Papathanasiou, S., and Hatziargyriou, N., "Dynamic modeling of microgrids," *International Conference on Future Power Systems*, pp. 1–7, Amsterdam, Netherlands, 18 November 2005.
30. Soutanis, N., Papathanasiou, S., and Hatziargyriou, N., "A stability algorithm for the dynamic analysis of inverter dominated unbalanced LV microgrids," *IEEE Trans. Power Syst.*, Vol. 22, pp. 294–304, February 2007.
31. Brucoli, M., Green, T., and McDonald, J., "Modelling and analysis of fault behaviour of inverter microgrids to aid future fault detection," *IEEE Conference on System of Systems Engineering*, pp. 1–6, San Antonio, TX, 16–18 April 2007.
32. Ong, C., *Dynamic Simulation of Electric Machinery Using MATLAB/Simulink*, Upper Saddle River, NJ: Prentice Hall, pp. 204–258, 1998.
33. Sauer, P., and Pai, M., *Power System Dynamics and Stability*, Champaign, IL: Stipes Publishing, pp. 215–270, 1997.
34. Erickson, M. J., and Lasseter, R. H., "Integration of battery energy storage element in a CERTS microgrid," *2010 IEEE Energy Conversion Congress and Exposition (ECCE)*, pp. 2570–2577, Phoenix, AZ, 12–16 September 2010.
35. Krishnamurthy, S., Jahns, T. M., and Lasseter, R. H., "The operation of diesel gensets in a CERTS microgrid," *2008 IEEE Power and Energy Society General Meeting—Conversion and Delivery of Electrical Energy in the 21st Century*, pp. 1–8, Pittsburgh, PA, 20–24 July 2008.

36. Nikkhajoei, H., and Lasseter, R., "Distributed generation interface to the CERTS microgrid," *IEEE Trans. Power Delivery*, Vol. 24, pp. 305–308, July 2002.
37. Wasynczuk, O., and Sudhoff, S., "Automated state model generation algorithm for power circuits and systems," *IEEE Trans. Power Syst.*, Vol. 11, pp. 1951–1956, November 1996.
38. Jatskevich, J., *A State Algorithm for the Automated State Model Generator*, Ph.D. Thesis, Purdue University, West Lafayette, IN, 1997.
39. Wasynczuk, O., Walters, E., and Hegner, H., "Simulation of a zonal electric distribution system for shipboard applications," *Energy Conversion Engineering Conference*, pp. 268–273, Honolulu, HI, 27 July–1 August 1997.
40. Krause, P., Wasynczuk, O., and Sudoff, S., *Analysis of Electric Machinery and Drive Systems*, Piscataway, NJ: IEEE Press, Chap. 11, pp. 395–425, 2002.
41. Zhao, Y., and Guo, L., "Dynamical simulation of laboratory microgrid," *Asia-Pacific Power and Engineering Conference*, pp. 1–5, Wuhan, China, 27–31 March 2009.
42. Lasseter, R., and Piagi, P., "Control and design of microgrid components," Tech. Rep. Publication 06-036, Power Systems Engineering Research Center, Madison, WI, January 2006.

### Appendix. Microgrid parameters

---

$r_1 = 18.9 \text{ m}\Omega$	$L_1 = 49.4 \text{ }\mu\text{H}$
$r_2 = 4.2 \text{ m}\Omega$	$L_2 = 5.9 \text{ }\mu\text{H}$
$r_3 = 47.4 \text{ m}\Omega$	$L_3 = 66.5 \text{ }\mu\text{H}$
$r_4 = 15.8 \text{ m}\Omega$	$L_4 = 22.2 \text{ }\mu\text{H}$
$r_{inv} = 12.8 \text{ m}\Omega$	$L_{inv} = 5 \text{ mH}$
$R_{load A} = 9.6 \text{ }\Omega$	$R_{load B} = 4.8 \text{ }\Omega$
$r_{TA(480 \text{ V})} = 10.2 \text{ m}\Omega$	$L_{TA(480 \text{ V})} = 135.9 \text{ mH}$
$r_{TA(208 \text{ V})} = 1.9 \text{ m}\Omega$	$L_{TA(208 \text{ V})} = 25.5 \text{ mH}$
$r_{TB(480 \text{ V})} = 17.1 \text{ m}\Omega$	$L_{TB(480 \text{ V})} = 226.6 \text{ mH}$
$r_{TB(208 \text{ V})} = 3.2 \text{ m}\Omega$	$L_{TB(208 \text{ V})} = 42.4 \text{ mH}$
$C_f = 3.2 \text{ }\mu\text{F}$	

---